Dynamic behavior of RC Frames against Progressive Collapse Subjected to Loss of a Corner Column Scenario

Jian-Fei Cheng[1], Qian Gu[1], Kai Qian[2], Feng Fu F. ASCE [3], Xiao-Fang Deng[2*]

[1]School of Civil Engineering and Architecture, Wuhan University of Technology, Wuhan, China, 430070.

[2]Guangxi Key Laboratory of Green Building Materials and Construction Industrialization, Guilin University of Technology, Guilin, China, 541004.

3 Department of Engineering, School of Science and Technology, City, University of London， Northampton Square, EC1V0HB

Abstract: In light of increasing concern about the progressive collapse of reinforced concrete (RC) structures, this study investigates the dynamic performance of RC frames against progressive collapse triggered by corner column removal. High-fidelity numerical models were built using software LS-DYNA. The model was validated through a comparison between numerical and experimental results. After this validation, a parametric analysis was conducted to explore the dynamic performance of structures following sudden corner column removal. A comparison was made between the load resistance and load transfer mechanisms of the RC frames under quasi-static and dynamic regimes. The effects of critical factors, such as strain rate and damping ratio, were discussed. Additionally, influences of slab thickness and the constraints from upper stories of the frame were also quantified. It was found that the energy-based method could effectively evaluate the dynamic resistance without inclusion of the effects of strain rate and damping ratio. It found that the effects of strain rate are negligible, while the damping ratio is crucial, as it reduces vibrations, peak displacement, and amplitude. The dynamic responses are greatly affected by the slab thickness. Meanwhile, the constraints from the upper floor of the frame can significantly mitigate the dynamic responses.

Keywords: progressive collapse; dynamic performance; numerical study; corner column.

* Corresponding author. E-mail address: dengxiaofang@glut.edu.cn

1. Introduction

Accidental events, such as gas explosions, vehicular impact, and terrorist attacks, may lead to the initial local failure of one or several structural components, ultimately resulting in the collapse of the entire structure or a disproportionately large part of it [1]. This phenomenon, known as "progressive collapse," has gained considerable attention since the catastrophic collapse of Ronan Point apartments in 1968. After the “911” events in 2001, studies on enhancing structural robustness against progressive collapse have gradually become a research focus in structural community [2-4]. Design methods for preventing progressive collapse can be categorized as indirect and direct design methods [5-6]. The alternative load path (ALP) method, a direct design method, assesses whether there are reliable alternative paths for load distribution of the remaining structure, regardless of accident events. This method is widely applied in progressive collapse studies [7-12].

Based on the ALP method, numerous studies had been carried out to investigate the load-resisting mechanisms of reinforced concrete (RC) structures against progressive collapse, such as compressive arch action (CAA) and tensile catenary action (TCA) for beam-column substructures[13-16], as well as compressive membrane action (CMA) and tensile membrane action (TMA) for beam-slab substructures [17-19]. Furthermore, the Vierendeel action (VA) has been observed in both multi-story two-dimensional and three-dimensional substructures [20,21]. Qian and Li **Error! Reference source not found.** studied the performance of three-dimensional beam-column substructures under a corner column missing scenario, the effects of various reinforcement details and span-to-height ratios on progressive collapse performance were discussed. Qian et al. [23] conducted quasi-static tests of three-dimensional RC substructures under an intenal column loss, evaluated the 3D and slab effects, and

discussed the secondary load-resisting mechanisms of RC frames with slabs. Sasani [24] conducted a study on the dynamic behavior of a 6-story RC frame, finding that Vierendeel action (VA) is the primary mechanism facilitating load redistribution when a corner column is lost. Qiao et al. [20] and Qian et al. [21] conducted studies on multi-story substructures, and found that the influence of the VA cannot be ignored. Additionally, the top and bottom floors exhibit different behavior to resist progressive collapse.

However, the majority of current studies on progressive collapse are based on quasi-static tests, mainly due to the difficulty of dynamic testing arrangement. But progressive collapse is a dynamic process caused by sudden column removal. To tackle this issue, Izzuddin et al. [25] proposed an energy-based method (EBM) that converts quasi-static responses into equivalent dynamic responses, utilizing the principle of energy conservation. Nonetheless, EBM may have some errors as the strain rate effects and damping ratio are ignored [26]. Additionally, the EBM requires the structure to exhibit the identical failure mode and load transfer mechanism under both quasi-static and dynamic conditions, which is still unsure [26,27] Furthermore, apart from other column removal scenarios, corner column removal may result in more severe consequence. This is because, in the event of a corner column removal, the structure heavily relies on flexural action to resist progressive collapse and ineffective in developing the TCA and TMA [7,28]. However, the dynamic behavior of spaced frames under sudden removal of a corner column scenario was still unclear. To fill this gap, high-fidelity finite element (FE) model of RC frame was developed based on the quasi-static test conducted by Feng et al. [7]. The accuracy of the numerical model was verified by test results. Subsequently, with the validated model, a series of dynamic analysis was performed under a sudden column removal scenario. The load resistance and load transfer mechanisms of the structure under quasi-static and dynamic methods were compared. The critical factors, such as the effects of strain rate and damping ratio, were discussed.

Moreover, parametric studies were conducted to examine the influence of slab thickness and the constraints from upper stories.

2. Numerical model set up

2.1. Previous experimental work

Feng et al. [7] performed an experiment on four half-scaled beam-slab substructures to investigate their resistance to progressive collapse initiated by corner column removal. The prototype building, illustrated in Fig. 1, was seismically designed following Chinese codes [29,30], featuring a ground story height of 3900 mm and an upper story height of 3600 mm, with a span of 5000 mm in both directions.

Specimen numbered as US from [7] was replicated in the numerical model . As depicted in Fig. 2, the overall dimensions of Specimen US were 3200 mm × 3200 mm, with a slab thickness of 70 mm, and cross-section of 300 mm × 300 mm and 100 mm × 250 mm for the column and beam, respectively. Fig. 3 illustrates the experimental setup of Specimen US. The column supports were anchored to the RC blocks, which in turn were bolted onto a robust floor. A dead load (DL) and live load (LL) of 5.5 and 2.0 kPa respectively, as well as an additional uniform load of 12.0 kN/m^2 were applied on the slabs' extended parts. This extra load was to simulate the additional constraints imposed by surrounding slabs in accordance with 2(DL+0.25LL) load combination recommended by GSA (2003) [31]. The experiment was loaded using a displacement-controlled concentrated loading method. The concrete exhibited an average cubic compressive strength of 26.6 MPa, equivalent to 21.3 MPa for the cylinder compressive strength. The characteristics of the rebar are detailed in Table 1. For further information, refer to Feng et al. [7].

2.2. Modeling details and methodology

The FE model is built and validated through the numerical software LS-DYNA. To circumvent the issue of divergence encountered during the large deformation stage, an explicit solver was employed. The geometrical model of Specimen US is demonstrated in Fig. 4.

2.2.1. Element type and material model

To significantly save computational time while maintaining acceptable accuracy, the eight-node solid element (*Element Solid 164) was adopted to model the concrete and steel plates using a reduced integration strategy. Meanwhile, a two-node Hughes-Liu beam element (*Element Beam 161), with a 2×2 Gauss quadrature integration, was employed for the simulation of rebars.

Material properties employed in the FE models are shown in Table 2. The concrete material was modeled using the continuous surface cap model (CSCM) for its numerical stability under both static and dynamic conditions [16,32]. While the model could dictate element failure based on the maximum principal strain, it exhibited limitations in simulating shear failure when this criterion was the sole determinant for the erosion criterion. Given the pronounced shear deformation at the beam ends, it became imperative to define the maximum shear strain with an erosion criterion *MAT_ADD_EROSION. A solid element is deleted at maximum principal strain or shear strain. LS-DYNA accommodates both a simplified and comprehensive version of the CSCM model, identified as *MAT_CSCM_CONCRETE and *MAT_CSCM, respectively. The simplified version is more user-friendly, requiring only three input parameters. However, the simplified CSCM is only applicable for unconfined compressive strength f_c' ranging from 28 MPa to 58 MPa. Given that the concrete strength of the Specimen US measured 21.3 MPa, the full version of the model was employed instead. Nonetheless, the default values tend to overstate the structural resilience and initial stiffness [32]. Therefore, to refine the numerical outcomes, adjustments were made to the fracture energy and elasticity modulus, in accordance with the recommendations provided by the model developer [33,34].

Rebars were modeled using the bilinear elastic-plastic material model (*MAT_PLASTIC_KINEMATIC). The model can be converted from kinematic hardening only (β =0), mixed hardening (β between 0 and 1) to isotropic hardening (β =1) by adjusting the hardening parameter β [35]. In this study, isotropic hardening is selected, assuming that the characteristics exhibited in tension are similar to those in compression. Material property parameters are derived from material coupon tests. The corresponding rebar element is automatically removed whenever the strain exceeds the assigned ultimate strain values, which are 0.18 for R6 and 0.23 for T12. It should be noted the strain rate effects were neglected for quasi-static test. Furthermore, the loading plate was modeled using a rigid material (*MAT_RIGID), while the other steel plates were modeled using linear elastic material (*MAT_ELASTIC).

2.2.2. Contact definition

The automatic single surface contact algorithm (*CONTACT_AUTOMATIC_SINGLE_SURFACE) was utilized for the face-to-face contact analysis. This algorithm calculates element contact in a penalty function manner and automatically checks for model penetration. Since there is no need to define contact and target surfaces, this algorithm is particularly useful in situations where the specific contact scenario cannot be predicted. Hence, the automatic single surface contact algorithm was strategically deployed to manage the contact interface between the loading plate and the concrete. Further, previous studies [36,37] have confirmed that neglecting bond-slip enable sufficient computational accuracy and simplifying the process, as the relative slip between rebars and concrete has a negligible impact on the overall results. Consequently, rebars are integrated into surrounding concrete with *CONSTRAINT_LAGRANGE_IN_SOLID. To balance result accuracy and computational cost, an element dimension of 20 mm is employed for concrete and rebar elements.

2.2.3. Boundary conditions and loading methodology

In the experiment setup, each supporting column was securely anchored to the foundation with bolts. In the numerical model, the foundation was simplified as a steel plate, with full constraints applied thereupon. Additionally, the heavy object placed on the extending slab was simplified as a uniform load on the corresponding slab. Simultaneously, to mitigate stress concentration, a loading plate was situated atop the corner column, with a one-way pin being strategically positioned between the loading plate and the jack, employing the keyword *CONSTRAINED_JOINT_REVOLUTE. Displacement-controlled loading was implemented with the keyword *BOUNDARY_PRESCRIBED_MOTION_SET.

2.3. Numerical model validation

Fig. 5 compares the load-displacement curve between the test and FE model. In the absence of adjacent components to constrain the corner column, the substructure mirrors the load-bearing characteristics of a cantilevered slab. Comprising solely the rising and softening segments, the load-displacement curve is accurately simulated by the numerical model. The discrepancy between the experimental and predicted critical values, including yield and peak load, remains insignificantly less than 6%. Fig. 6 compares the failure modes from the experimental test and numerical model. It is evident that the numerical model precisely reflects the failure characteristics of Specimen US: plastic hinges appear at the far end of the adjacent beam to the failed corner column, the bottom concrete of the beam is crushed, and the corresponding area of the rebar yields. Simultaneously, the main crack forms along the diagonal direction of the slab surface, indicating that the model successfully predicts the manner of test failure.

Test results confirms the accuracy of the numerical model. Consequently, this model will serve as the benchmark model for developing dynamic models in the subsequent analysis.

3. Dynamic analysis of RC frames against progressive collapse

3.1. Methodology for dynamic modeling

Fig. 7 presents the numerical model for dynamic analysis, different to quasi-static model, as illustrated in Fig. 8, the loading scheme for dynamic analysis involves a three-step process to simulate the scenario of sudden column loss. First, self-weight and external loads are applied using the keyword *LOAD_BODY_Y with a gravity acceleration of 9.8 m/s^2, corresponding to the period from 0 to T_1. Then, an additional period (T_1 to T_2) was introduced to mitigate possible dynamic vibration from the load applied at the initial step (0 to T_1). Following this, at time T_2, the column removal was executed by eroding the steel plate under corner column using the keyword of *MAT_ADD_EROSIO. The support of corner column was released within a one-time step, corresponding to a time increment of 3.4×10^{-4} s, resulting in a practically nearly instantaneous removal column by the explosion. The density within the corresponding regions of the structure was scaled using the keyword *ELEMENT_MASS to consider the external loads more realistically [37].

3.2. Comparison between static and dynamic analysis

3.2.1. Load resistance

As illustrated in Fig. 9, according to the EBM put forth by Izzuddin et al. [25], if the remaining structure regains equilibrium after the initial failure, the external work ($P_d \cdot u_d$) from gravity should equal the strain energy ($\int_0^{u_d} P_{NS}(u)du$) within the remaining structure, in accordance with the conservation of energy. Through the conversion of the structure's quasi-static resistance into dynamic

resistance, the corresponding dynamic progressive collapse resistance (P_d) under displacement (u_d) can be ascertained.

As shown in Fig. 10(a), the incremental dynamic analysis (IDA) reveals a rising trend in the vertical peak displacement of the target column, coinciding with the increase in external load. Once the load exceeds 34.0 kN, the remaining structure does not maintain stability and eventually fails. Therefore, the dynamic ultimate strength of the building is 34.0 kN. It should be noted that the EBM did not consider the effects of strain rate and damping ratio.

Fig. 10(b) compares the structural load resistance between EBM and IDA. Each point in the IDA curve represents a nonlinear dynamic analysis. It is observable that the IDA curve agrees with EBM curve well although the values in IDA curve are slightly lower than that from EBM curve. For example, the dynamic ultimate strength obtained by the EBM and the IDA is 36.9 kN and 34.0 kN, respectively, with only a 7.9% difference. The results demonstrate that the EBM, as a simplified assessment method, can accurately assess the dynamic resistance of the structure excluding the effects of strain rate and damping ratio.

3.2.2. Failure mode

One critical assumption for using EBM is the consistency of failure modes whether subjected to quasi-static or dynamic load regime. Fig. 11 compares the failure modes at displacements of 84 mm and 500 mm, representing peak and residual resistances under quasi-static analysis, in both loading scenarios. In either loading regime, the main cracks appear along the diagonal of the slab before failure, with noticeable cracks also evident on Beams AD and AB. With further displacement of the corner column, the cracks propagate along the diagonal, culminating in the emergence of plastic hinges and eventual structural collapse. Thus, the failure modes and load transfer mechanisms are consistent across both loading regimes throughout the whole loading process.

3.3. Discussion on effects of strain rate and damping ratio

This section explores the impact of critical factors, such as strain rate and damping ratio, which are crucial in evaluating the structural dynamic performance during progressive collapse.

3.3.1. Influence of strain rate

In the numerical models, an "IRATE" parameter value of 1 was set for the CSCM model to define the rate-dependent stress-strain relationship, highlighting the increased strength of concrete at high strain rates [33]. The rate effect formulations are drawn from Simo's extension [38] of the popular Duvaut-Lions formulation. According to model developers [34], the fracture energy should be reduced (REP0W=0.5) if noticeable shear or compression damage was present. The Cowper-Symonds model was employed to simulate the strain rate effects of the rebar in this material model [39], with strain rate parameters C and P defined as 40.4 s^{-1} and 5, respectively [40,41].

To explore the influences of the strain rate, four cases were examined using IDA: Case 1 ignored strain rate effects; Case 2 only considered strain rate effects of rebar; Case 3 account strain rate effects of concrete only; and Case 4 considered strain rate effects of both rebar and concrete. Fig. 12 indicates minor differences among the four cases during the elastic stage, with the significant increase in strength manifesting primarily in the plastic stage. The strain rate effects of rebar have a more noticeable impact than those of concrete, aligning with prior studies on RC slabs by Russell et al. [42] and Ding et al. [43]. The four cases correspond to dynamic ultimate strengths of 34.0 kN, 36.0 kN, 34.5 kN, and 40.0 kN. Compared to Case 1, the corresponding deviations are 2.9%, 1.5%, and 4.4%, respectively. This is because the impact of strain rate is relatively limited due to the low strain rate observed during sudden column removal.

3.3.2. Influence of damping ratio

In this study, the keyword *DAMPING_GLOBAL was employed to implement Rayleigh damping, and the structural damping ratio ζ was defined utilizing the concept of logarithmic decrement. However, as no dynamic tests were carried out and the damping ratio could not be obtained from the real dynamic responses, a critical damping ratio of 5% was implemented as recommended for general RC constructions [26]. To explore the influence of damping ratio on dynamic responses, additional damping ratios of 0, 1%, and 2% were also evaluated. For comparison, strain rate effects were disregarded in this section.

As shown in Fig. 13(a), at lower external loads, damping ratios show little effect on displacement responses. However, with an increase in external load, these responses start to differ noticeably. An increase in damping ratio from 0 to 5% results in a rise in dynamic ultimate strength from 34.0 kN to 38.5 kN, signifying a 13.2% increase. This suggests that structural damping ratio plays a considerable role in the prevention of structural dynamic collapse.

Fig. 13(b) demonstrates the structural dynamic responses under a 30.0 kN external load with varying damping ratios. As damping ratio increases from 0 to 5%, the vertical peak displacement decreases from -75.1 mm to -53.0 mm, resulting in a reduction of 29.4%. The results show that damping helps to diminish vibrations and simultaneously lessening the peak displacement and magnitude of vibrations. Hence, for significant constructions, the implementation of dampers can bolster the structure's capability to resist collapse.

4. Parametric study on building layout

For a thorough examination of the dynamic behavior of RC frames in mitigating progressive collapse, a parametric study was further conducted. It is noteworthy that due to experimental

limitations, the test specimens simplified the boundary conditions of the structures and did not consider the horizontal constraints from the floor slabs around the corner area. Additionally, the supporting columns were simplified to short columns of 700 mm in height, rather than their actual length. To mitigate the adverse effects of these simplifications on the results, two-bay by two-bay structures with full-length columns, named US-1F and US-2F, were modeled, as shown in Fig. 14. It should be noted that 1F and 2F denote one-story and two-story, respectively. Moreover, to better simulate the actual structural loading, a uniform load was employed on the floor panels instead of a concentrated load in the following study.

4.1. Effects of slab thickness

Following the US model, the effects of slab thickness on the dynamic responses are investigated by both decreasing and increasing the slab thickness, while maintaining the identical slab reinforcement ratios as those used in the US model. It is noteworthy that all the reinforcement ratios for slabs with varying thicknesses were in compliance with the guidelines for minimum and maximum reinforcement ratios. Given a beam depth of 250 mm, the examined slab thickness of 50 mm, 60 mm, 70 mm and 80 mm represent slab thickness-to-beam depth ratios of 0.20, 0.24, 0.28 and 0.32, respectively. It is worth noting that the design service loads (DL + 0.25LL), which are equivalent to 6.0 kPa, were applied to the floor slabs.

Fig. 15(a) demonstrates the effects of slab thickness on structural dynamic responses. As the slab thickness increased from 50 mm to 80 mm, the peak displacement decreased from -16.2 mm to -11.7 mm. This indicates that the slab thickness significantly affects the structural dynamic response. Nevertheless, since the load is relatively small, the structure is almost at the elastic deformation stage,

with CAA occurring within the beams depicted in Fig. 15(b). This indicates that under the design service loads, the structure exhibits strong resistance to progressive collapse.

4.2. Effects of constraints from upper stories

In this study, the surface atop the corner column of a single-story frame substructure is taken as a free end. However, in practice, for multi-story frame structures, the surface atop the corner column is subject to constraints from the upper floor. Previous studies based on static analysis [16,44] have demonstrated that multi-story frames can redistribute vertical loads through interlayer action (also known as VA). However, the effects of the VA on the dynamic responses of the frames are unclear. Thus, a two-story frame structure, referred to as US-2F, was devised, wherein equal loads were applied to both the upper and lower floors.

Fig. 16(a) compares displacement response under different loads for both US-1F and US-2F, it was found that vertical peak displacement of US-2F decreased by 39.5%, 44.4%, and 56.6% respectively in accordance with the loads of 6.0 kPa, 12.0 kPa, and 18.0 kPa. This indicates that the constraint effects of the upper floor can significantly reduce the structural dynamic response, and these effects become more significant as the external load increases. Furthermore, as illustrated in Fig. 16(b), before column removal, the corner column is subjected to compressive axial force, with load being transferred from the upper to the lower floor. Once the column is removed, the force shifts to tension indicating vertical movement constraint by the upper floor, thereby reducing dynamic responses.

Fig. 16(c) presents time-history of axial force in the beam cross-sections under various constraints with the design service loads of 6.0 kPa. Sections X and Y, situated close to columns D and A on Beam AD respectively, have been selected for this analysis. It should be noted that the terms US-1F-X and US-2F-X designate the X cross-section of US-1F and X cross-section of the bottom floor in US-2F,

respectively. After the column is removed, both sides of Beam AD are in compression. For the US-1F model, the stable axial compression force amounts to 55.1 kN and 2.1 kN for sections X and Y respectively. In contrast, the US-2F model records axial forces of 43.1 kN and 13.1 kN in sections X and Y respectively, indicating a more uniform axial load distribution owing to the constraints imposed by the upper floor. This behavior can be attributed to the development of VA in redistributing load, which can be characterized by the shear forces of the corner column (see Fig. 16(d)). This leads to a more uniform load distribution across multi-story structures, thereby enhancing structural resilience against collapse.

5. Conclusions

In this investigation, high-fidelity FE numerical models were utilized to study the dynamic response of RC frames against progressive collapse caused by a corner column removal scenario. Based on numerical and parametric analysis, the following conclusions can be drawn:

1. The LS-DYNA software could simulate the failure mode of RC frames subject to corner column failure reasonably, including concrete crushing/spalling and crack patterns in slabs.
2. Both quasi-static and dynamic analysis results demonstrate a consistent behavior in terms of failure modes and load transfer mechanisms, irrespective of the loading regime. The energy-based method effectively evaluates structural dynamic resistance without considering the effects of strain rate and damping ratio.
3. The parametric analysis showed that the strain rate effects are negligible, and overlooking this factor may result in conservative outcomes. On the other hand, damping ratio plays a crucial role in structural collapse; it not only aids in the decay of vibrations but also diminishes the peak displacement and amplitude of vibrations.

4. Slab thickness substantially affects dynamic responses, and the structure exhibits strong anti-progressive collapse performance under design service loads. The constraints from upper stories in multi-story frame structures reduce dynamic responses and enhance structural robustness.

6. Acknowledgments

This research was supported by a research grant provided by the Natural Science Foundation of Guangxi, China (No.2021GXNSFFA196001), National Natural Science Foundation of China (Nos. U22A20244 and 52022024). Any opinions, findings and conclusions expressed in this paper do not necessary reflect the view of National Natural Science Foundation of China and Natural Science Foundation of Guangxi, China.

References

[1] ASCE/SEI 7, Minimum design loads for buildings and other structures, Reston (VA): Structural Engineering Institute, ASCE, 2010.

[2] Kiakojouri F, De Biagi V, Chiaia B, Sheidaii M R, Progressive collapse of framed building structures: Current knowledge and future prospects, Eng. Struct. 206 (2020), 110061.

[3] Azim I, Yang J, Bhatta S, Wang F L, Liu Q F, Factors influencing the progressive collapse resistance of RC frame structures, J. Build. Eng. 27 (2020), 100986.

[4] Pang B, Wang F, Yang J, Nyunn S, Azim I, Performance of slabs in reinforced concrete structures to resist progressive collapse, Struct. 33 (2021), 4843-4856.

[5] DoD, Design of buildings to resist progressive collapse, UFC 4-023-03, U.S. Department of Defense, Washington, 2016.

[6] GSA, Progressive collapse analysis and design guidelines for new federal office buildings and major modernization projects, U.S. General Services Administration, Washington, 2016.

[7] Feng P, Qiang H, Ou X, Qin W H, Yang J X, Progressive collapse resistance of GFRP-strengthened RC beam–slab subassemblages in a corner column–removal scenario, J. Compos. Constr. 23(1) (2019), 04018076.

[8] Qian K, Lan X, Li Z, Li Y, Fu F, Progressive collapse resistance of two-story seismic configured

steel sub-frames using welded connections, J. Constr. Steel Res. 170 (2020), 106117.

[9] Qian K, Liang S L, Xiong X Y, Fu F, Fang Q, Quasi-static and dynamic behavior of precast concrete frames with high performance dry connections subjected to loss of a penultimate column scenario, Eng. Struct. 205 (2020), 110115.

[10] Liang S L, Li Z, Wang C L, Qian K, Experimental and analytical study on the compressive arch action of precast concrete assemblies with monolithic connections to resist progressive collapse, J. Struct. Eng. 149(4) (2023), 04023010.

[11] Lu X Z, Lin K Q, Li Y, Guan H, Ren P Q, Zhou Y L, Experimental investigation of RC beam-slab substructures against progressive collapse subject to an edge-column-removal scenario, Eng. Struct. 149 (2017), 91-103.

[12] Li S, Shan S D, Zhai C H, Xie L L, Experimental and numerical study on progressive collapse process of RC frames with full-height infill walls, Eng. Fail. Anal. 59 (2016), 57-68.

[13] Zhou Y, Chen T P, Pei Y L, Hwang H J, Hu X, Yi W J, Deng L, Static load test on progressive collapse resistance of fully assembled precast concrete frame structure, Eng. Struct. 200 (2019), 109719.

[14] Jin L, Lan D Q, Zhang R B, Li J, Qian K, Performance of RC beam-column assemblies during and after elevated temperature to resist progressive collapse, Eng. Struct. 283 (2023), 115802.

[15] Jin L, Lan D, Zhang R, Qian K, Effect of fire on behavior of RC beam-column assembly under a middle column removal scenario, J. Build. Eng. 67 (2023), 105496.

[16] Qian K, Weng Y H, Fu F, Deng X F, Numerical evaluation of the reliability of using single-story substructures to study progressive collapse behaviour of multi-story RC frames, J. Build. Eng. 33 (2021), 101636.

[17] Qian K, Wang D F, Huang T, Weng Y H, Initial damage and residual behavior of RC beam-slab structures following sudden column removal - numerical study, Struct. 36 (2022), 650–664.

[18] Dat P X, Hai T K, Membrane actions of RC slabs in mitigating progressive collapse of building structures, Eng. Struct. 55 (2013), 107-115.

[19] Yu J, Tang J H, Luo L Z, Fang Q, Effect of boundary conditions on progressive collapse resistance of RC beam-slab assemblies under edge column removal scenario, Eng. Struct. 225 (2020), 111272.

[20] Qiao H, Yang Y, Zhang J, Progressive collapse analysis of multistory moment frames with

varying mechanisms, J. Perform. Constr. Facil. 32(4) (2018), 04018043.

[21] Qian K, Cheng J F, Weng Y H, Fu F, Effect of loading methods on progressive collapse behavior of RC beam-slab substructures under corner column removal scenario, J. Build. Eng. 44 (2021), 103258.

[22] Yi W J, He Q F, Xiao Y, Kunnath S K, Experimental study on progressive collapse-resistant behavior of reinforced concrete frame structures, ACI Struct. J. 105(4) (2008), 433-439

[23] Qian K, Li B, Ma J X, Load-carrying mechanism to resist progressive collapse of RC buildings. J, Struct. Eng. 141(2) (2015), 4014107.

[24] Sasani M, Response of a reinforced concrete infilled-frame structure to removal of two adjacent columns, Eng. Struct. 30(9) (2008), 2478–2491.

[25] Izzuddin B A, Vlassis A G, Elghazouli A Y, Nethercot D A, Progressive collapse of multi-storey buildings due to sudden column loss—Part I: Simplified assessment framework, Eng. Struct. 30(5) (2008), 1308-1318.

[26] Pham A T, Tan K H, and Yu J, Numerical investigations on static and dynamic responses of reinforced concrete sub-assemblages under progressive collapse, Eng. Struct. 149 (2017), 2-21.

[27] Qian K, Liang S L, Xiong X Y, Fu F, Fang Q, Quasi-static and dynamic behavior of precast concrete frames with high performance dry connections subjected to loss of a penultimate column scenario, Eng. Struct. 205 (2020), 110115.

[28] Lim N S, Tan K H, Lee C K, Experimental studies of 3D RC substructures under exterior and corner column removal scenarios, Eng. Struct. 150 (2017), 409-427.

[29] Ministry of Housing and Urban-Rural Development of the People's Republic of China (MOHURD), Code for design of concrete structures, GB50010-2010. Beijing, China; 2010 (in Chinese).

[30] Ministry of Housing and Urban-Rural Development of the People's Republic of China (MOHURD), Code for seismic design of buildings, GB50011-2010. Beijing, China; 2010 (in Chinese).

[31] GSA, Progressive collapse analysis and design guidelines for new federal office buildings and major modernization projects, U.S. General Service Administration, Washington, 2003.

[32] Yu J, Luo L Z, and Li Y, Numerical study of progressive collapse resistance of RC beam-slab substructures under perimeter column removal scenarios, Eng. Struct. 159 (2018), 14-27.

[33] Murray Y D, User's manual for LS-DYNA concrete material model 159, United States. Federal Highway Administration. Office of Research, Development, and Technology, 2007.

[34] Murray Y D, Abu-Odeh A Y, Bligh R P, Evaluation of LS-DYNA concrete material model 159, United States. Federal Highway Administration. Office of Research, Development, and Technology, 2007.

[35] Hallquist J O, LS-DYNA keyword user's manual, Livermore Software Technology Corporation, 2007, 970.

[36] Qian K, Chen X Y, Huang T, Dynamic response of RC beam-slab substructures following instantaneous removal of columns, J. Build. Eng. 45 (2022), 103554.

[37] Yu J, Gan Y P, Liu J, Numerical study of dynamic responses of reinforced concrete infilled frames subjected to progressive collapse, Adv. Struct. Eng. 24(4) (2020), 635-52.

[38] Simo J C, Kennedy J G, Govindjee S, Non-smooth multisurface plasticity and viscoplasticity. Loading/unloading conditions and numerical algorithms, Int. J. Numer. Methods Eng. 26(10) (1988), 2161-2185.

[39] Cowper G R, Symonds P S, Strain hardening and strain rate effects in the impact loading of cantilever beams, Applied Mathematics Report, Brown University, 1958.

[40] Li L L, Li G Q, Jiang B H, Lu Y, Analysis of robustness of steel frames against progressive collapse, J. Constr. Steel Res. 143 (2018), 264-278.

[41] International Atomic Energy Agency, Safety aspects of nuclear power plants in human induced external events: assessment of structures, International Atomic Energy Agency: Vienna, Austria, 2018.

[42] Russell J M, Owen J S, Hajirasouliha I, Dynamic column loss analysis of reinforced concrete flat slabs, Eng. Struct. 198 (2019), 109453.

[43] Ding L, Van Coile R, Botte W, Gaspeele Robby, Quantification of model uncertainties of the energy-based method for dynamic column removal scenarios, Eng. Struct. 237 (2021), 112057.

[44] Tan Z, Zhong W, Tian L, Zheng Y H, Meng B, Duan S C, Numerical study on collapse-resistant performance of multi-story composite frames under a column removal scenario, J. Build. Eng. 44 (2021), 102957.

Captions of tables

426 **Table 1** Rebar properties

427 **Table 2** Material properties of concrete and rebar

428

429 **Captions of figures**

430 **Fig. 1.** Prototype structure (unit: in mm): (a) elevation; (b) floor plan

431 **Fig. 2.** Dimensions and reinforcement detailing of Specimen US (unit: in mm) [7]

432 **Fig. 3.** Test setup [7]

433 **Fig. 4.** Geometrical model of Specimen US

434 **Fig. 5.** Load-displacement curve

435 **Fig. 6.** Failure modes: (a) test [7]; (b) FE model

436 **Fig. 7.** Numerical model for dynamic analysis

437 **Fig. 8.** Loading scheme for dynamic analysis

438 **Fig. 9.** Illustration of energy-based method

439 **Fig. 10.** Response of dynamic analysis: (a) time-history response of displacement; (b) comparison
440 between EBM and IDA

441 **Fig. 11.** Comparison of failure modes under static and dynamic analysis

442 **Fig. 12.** Influence of strain rate on dynamic resistance

443 **Fig. 13.** Influence of damping ratio: (a) dynamic resistance; (b) time-history response of
444 displacement

445 **Fig. 14.** Numerical models for parametric studies: (a) US-1F; (b) US-2F

446 **Fig. 15.** Effect of slab thickness: (a) time-history response of displacement; (b) time-history of
447 beam axial force

448 **Fig. 16.** Effect of constraints from upper stories: (a) displacement; (b) axial force in the corner
449 column; (c) axial force in the beam with 6.0 kPa external load; (d) shear force in the corner column.

450

451 **Table 1** Rebar properties

Rebar	Diameter (mm)	Yield Strength (MPa)	Ultimate Strength (MPa)	Yield Strain (με)	Elongation Ratio (%)
R6	6	324	525	1543	23
T12	12	427	530	2135	18

Table 2 Material properties of concrete and rebar

Material	Model	Parameter	Magnitude	Unit
Concrete	*MAT_CSCM	Unconfined Compressive Strength	21.3	MPa
		Mass Density	2320	kg/m^3
		Maximum Principal Strain	0.08	-
		Maximum Shear Strain	0.3	-
Rebars	*MAT_PLASTIC_KINEMATIC	Yield Strength	324/427	MPa
		Ultimate Strength	525/530	MPa
		Mass Density	7850/7850	kg/m^3
		Elastic Modulus	210/200	GPa
		Poisson's Ratio	0.3/0.3	-
		Failure Strain	0.23/0.18	-

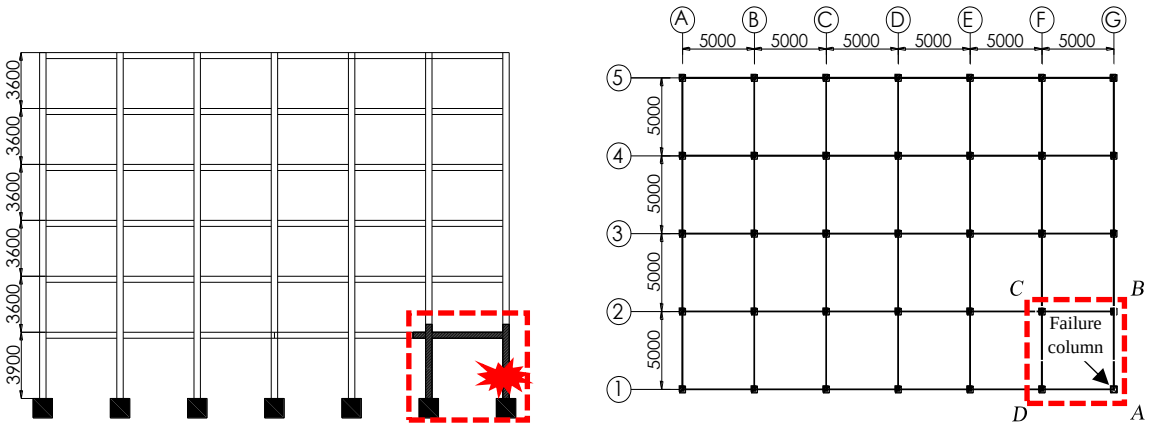

(a) (b)

Fig. 1 Prototype structure (unit: in mm): (a) elevation; (b) floor plan

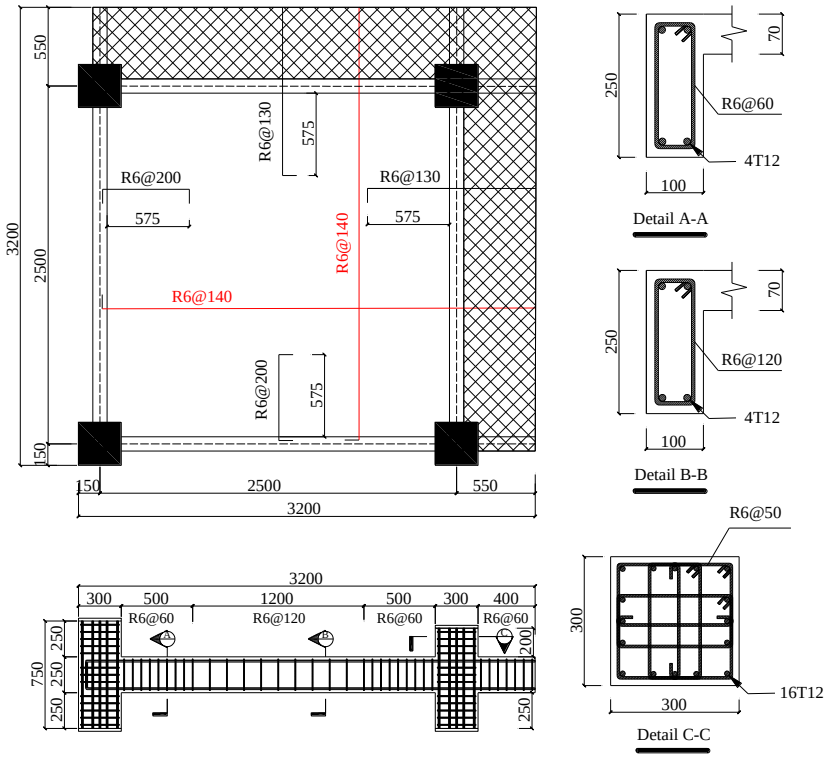

459

460 **Fig. 2** Dimensions and reinforcement detailing of Specimen US (unit: in mm) [7]

461

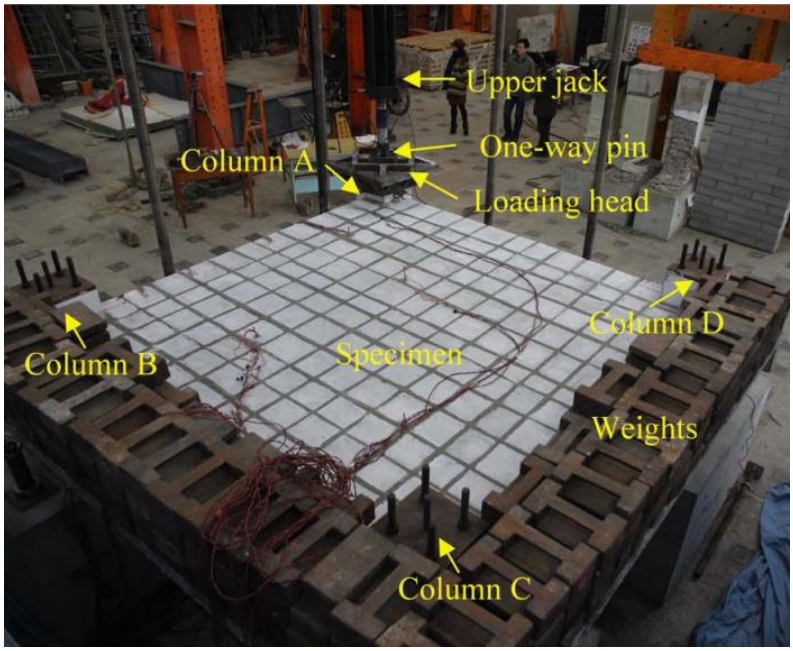

462

463 **Fig. 3** Test setup [7]

464

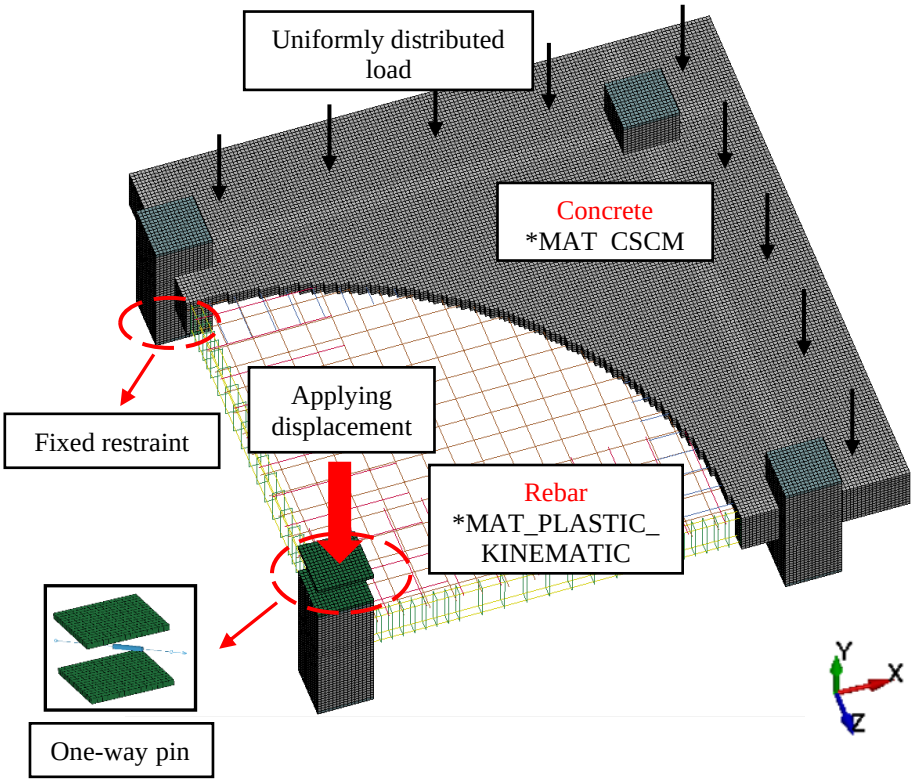

Fig. 4 Geometrical model of Specimen US

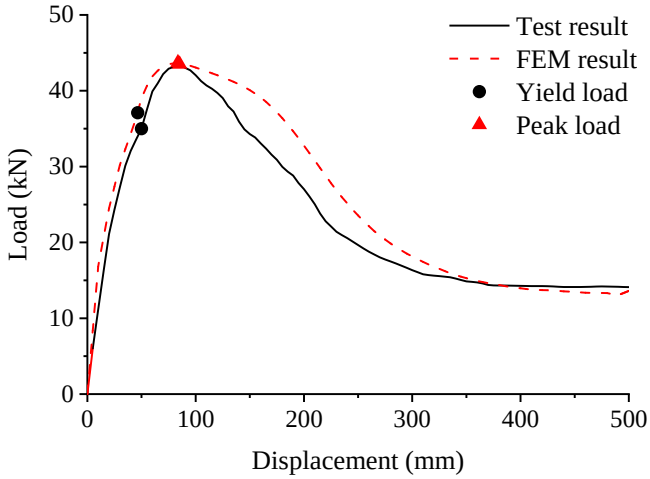

Fig. 5 Load-displacement curve

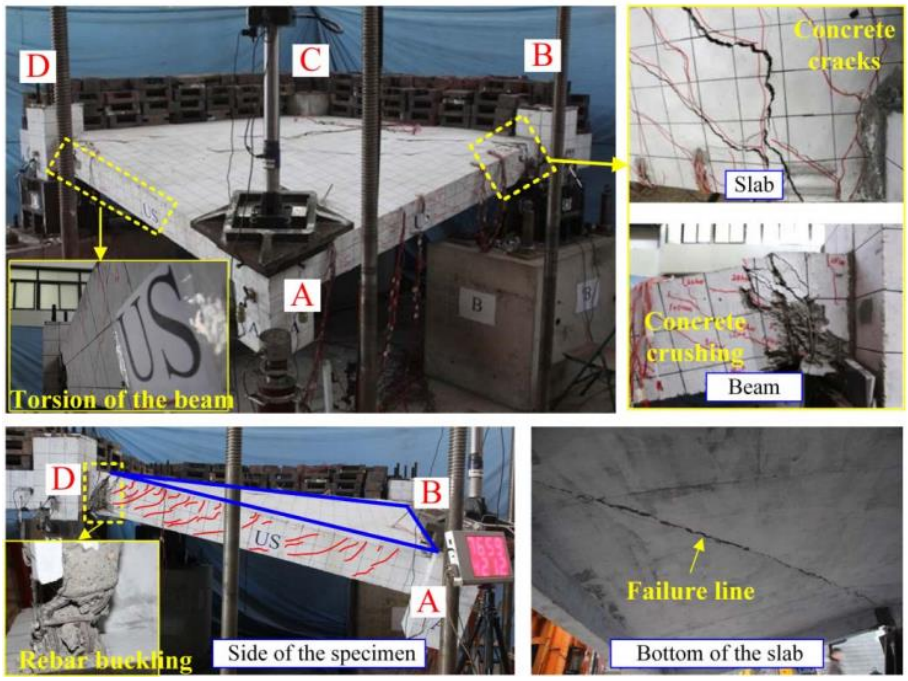

(a)

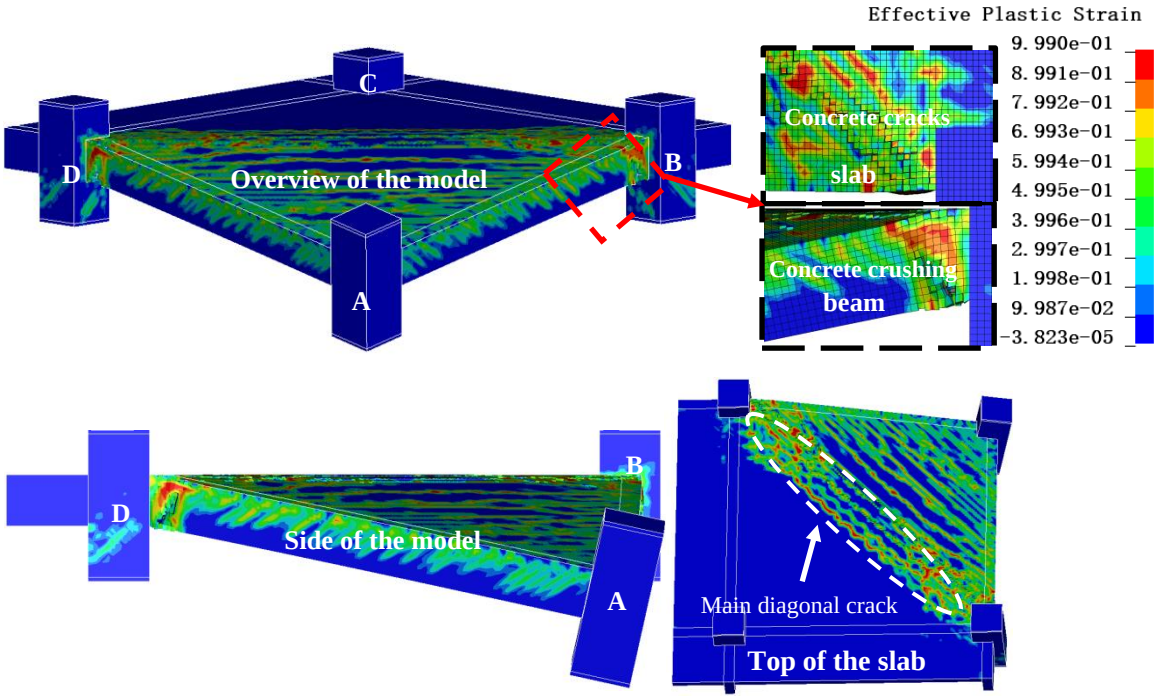

(b)

Fig. 6 Failure modes: (a) test [7]; (b) FE model

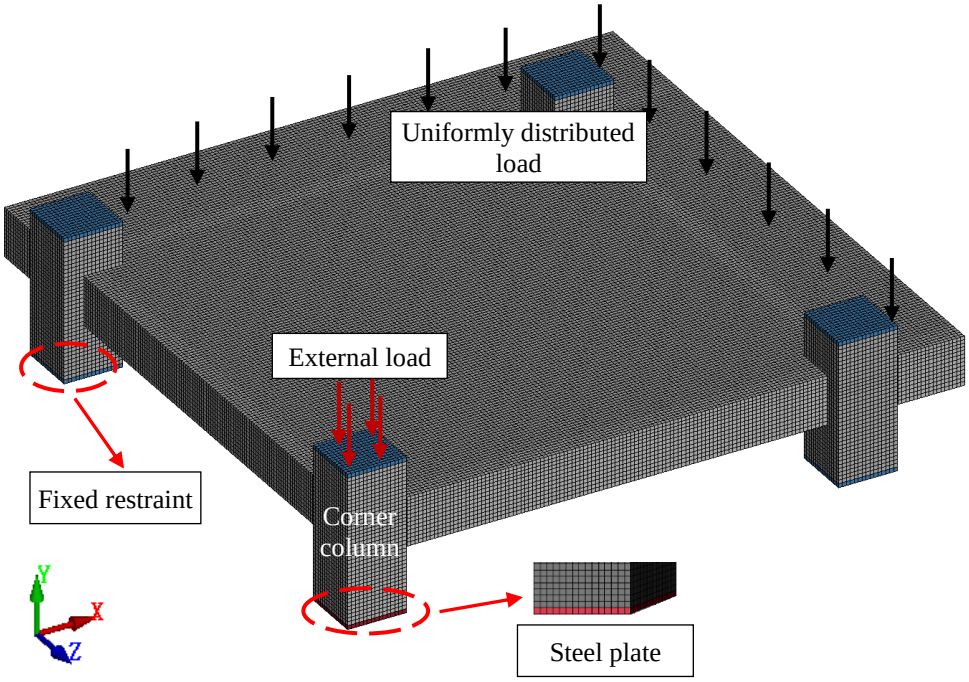

Fig. 7 Numerical model for dynamic analysis

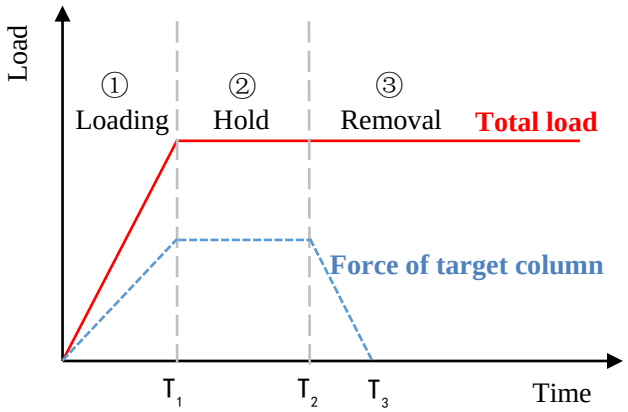

Fig. 8 Loading scheme for dynamic analysis

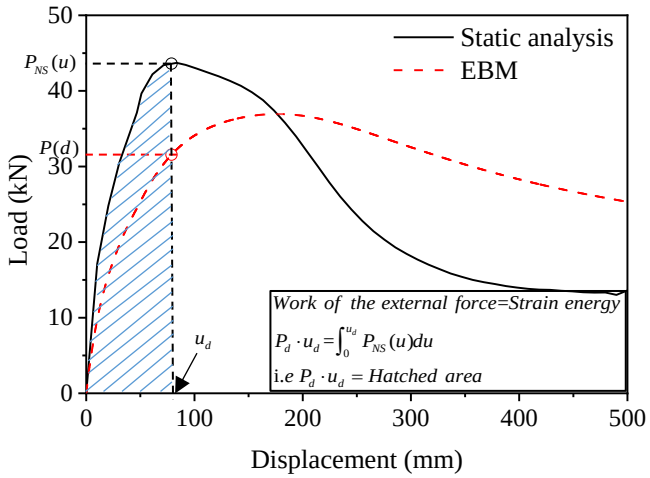

Fig. 9 Illustration of energy-based method

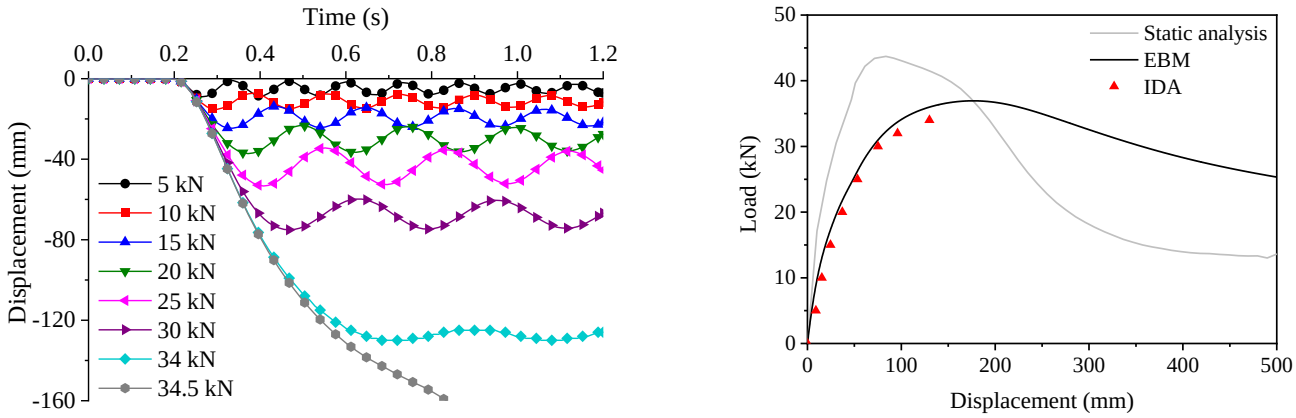

(a) (b)

Fig. 10 Response of dynamic analysis: (a) time-history response of displacement; (b) comparison between EBM and IDA

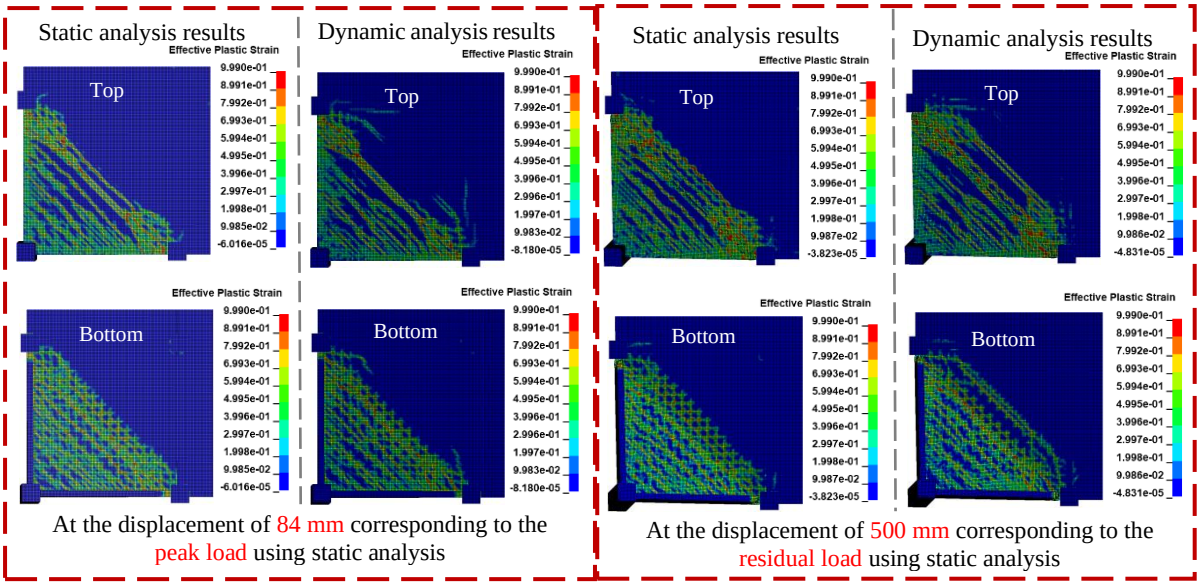

Fig. 11 Comparison of failure modes under static and dynamic analysis

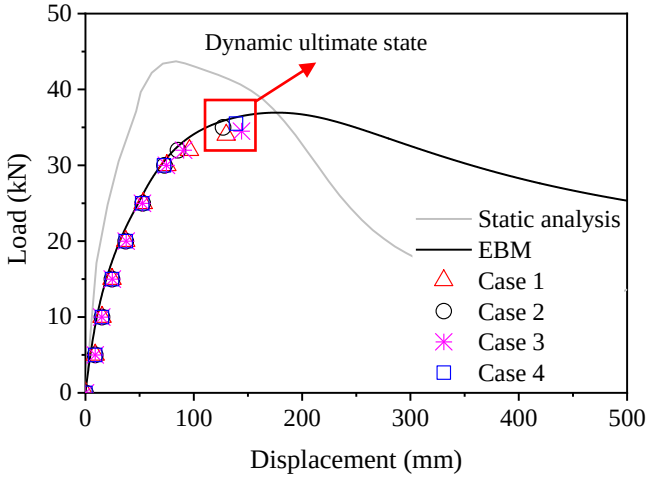

Fig. 12 Influence of strain rate on dynamic resistance

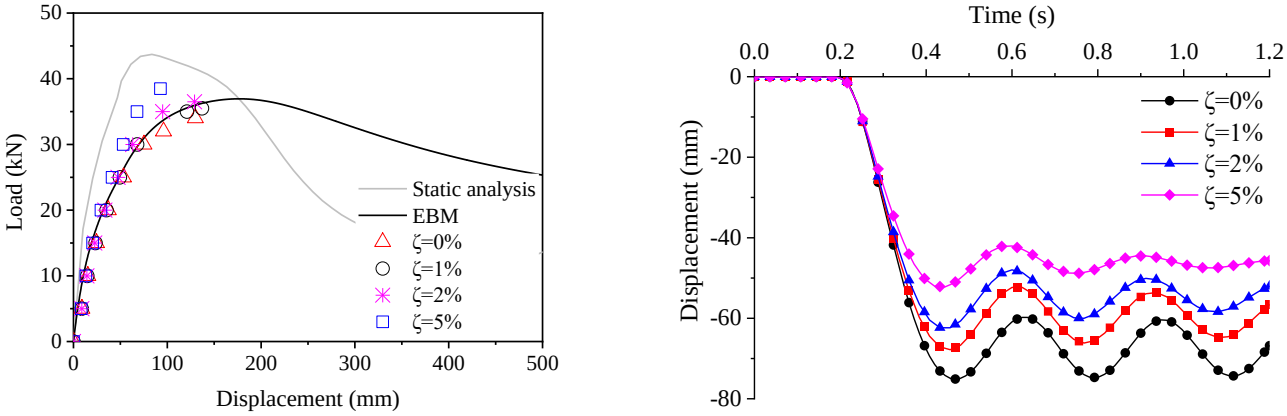

(a) (b)

Fig. 13 Influence of damping ratio: (a) dynamic resistance; (b) time-history response of displacement

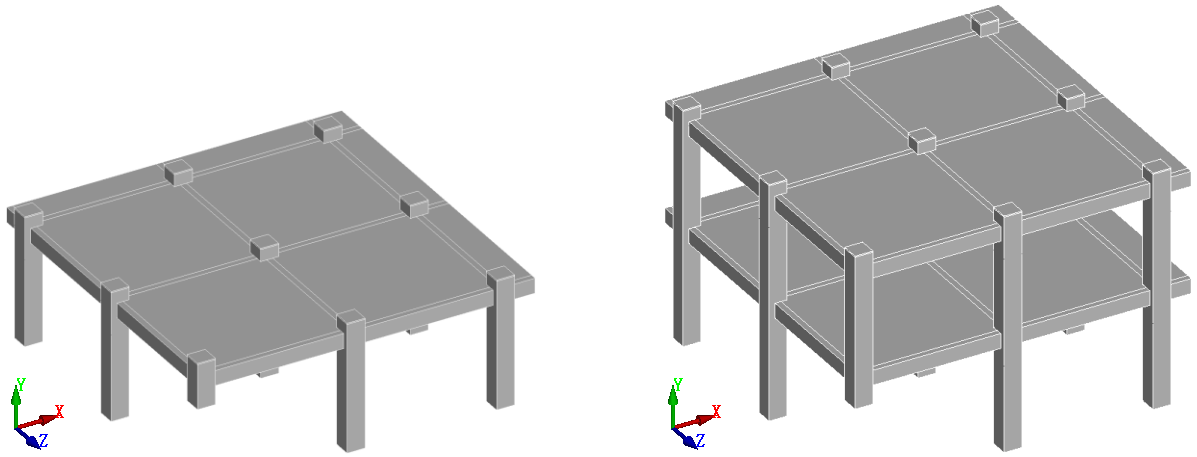

(a) (b)

Fig. 14 Numerical models for parametric studies: (a) US-1F; (b) US-2F

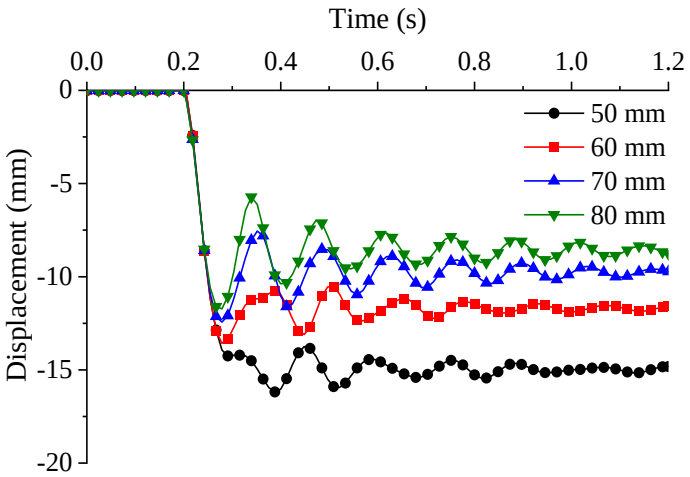

(a)

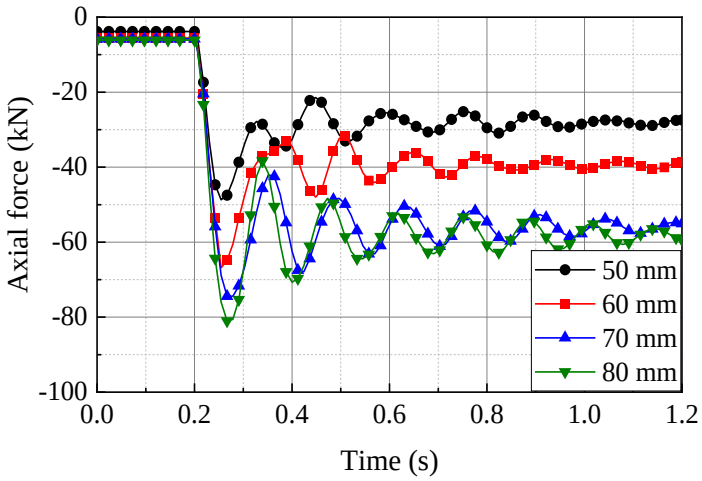

(b)

Fig. 15 Effect of slab thickness: (a) time-history response of displacement; (b) time-history of beam axial force

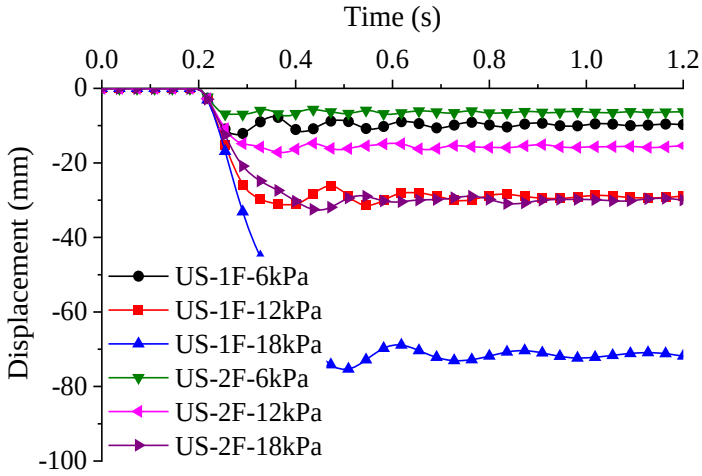

(a)

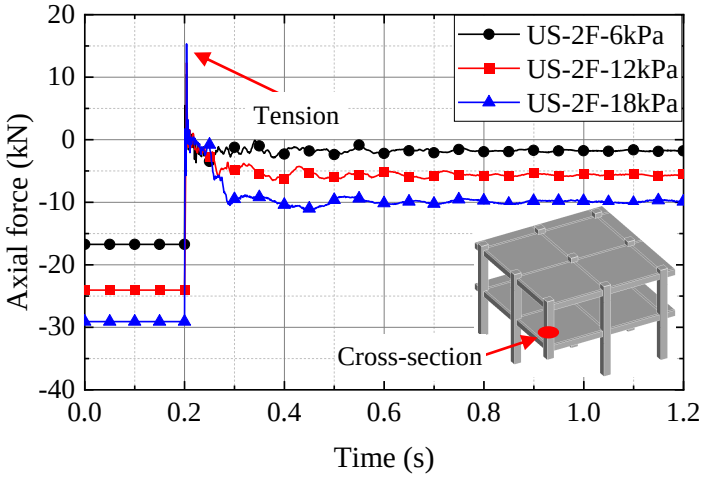

(b)

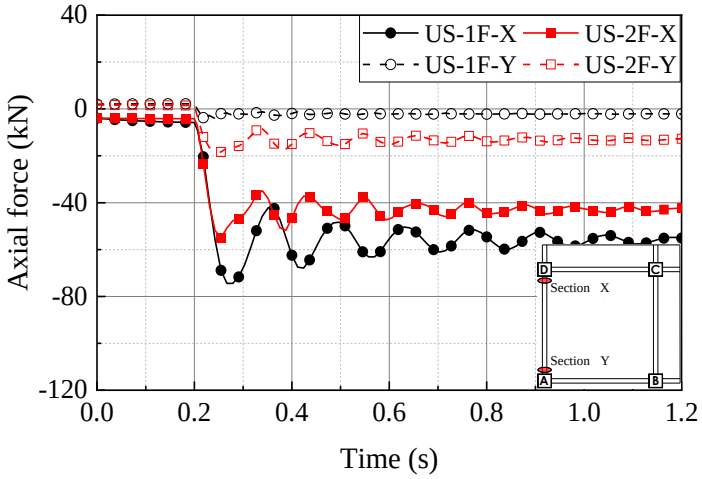

507

508 (c)

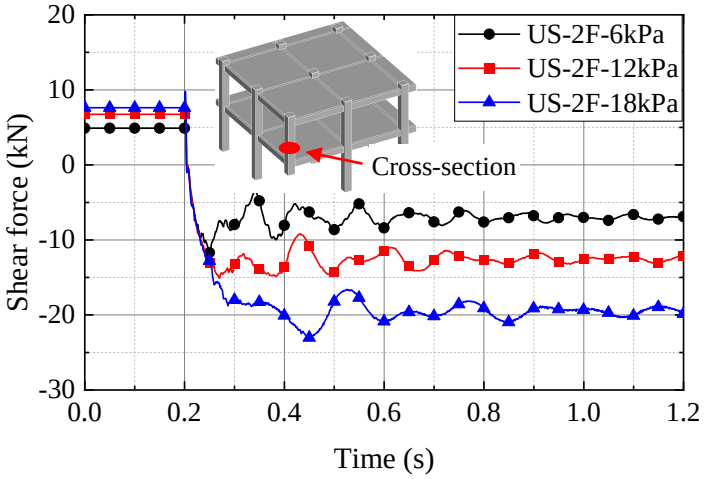

509

510 (d)

511 **Fig. 16** Effect of constraints from upper stories: (a) displacement; (b) axial force in the corner

512 column; (c) axial force in the beam with 6.0 kPa external load; (d) shear force in the corner column.